Master thesis

**Master's degree in Industrial Engineering**

# Image gradient based 3D roughness estimation and rendering for haptic palpation from a single skin image

*Department of Information & Telecommunication Engineering, Incheon National University, Incheon, Republic of Korea.*

*Barcelona School of Industrial Engineering, Polytechnic University of Catalonia, Barcelona, Catalonia, Spain.*

Autor: Julia Ibanez Vicente

Director: Kwangtaek Kim

**Abstract**

**Background/purpose:** Skin palpation and property analysis (roughness, dryness, stiffness, temperature) are crucial for skin examination and diagnose. That is why is needed a noncontact-based method that allows to carry it out avoiding secondary infections or damage. A haptic device with haptic feedback was designed some years ago, but accurate results for 3D skin surface reconstruction and roughness estimation are still in research and improvement. In this study is proposed a gradient-based skin surface 3D roughness estimation algorithm that will enable haptic palpation and roughness examination.

**Methods:** 3D roughness is estimated from 2D single image. First step is pre-processing the image, to improve the quality and reduce the noise by using contrast stretching and bilateral filtering. After, the gradient field is computed and used to obtain the 3D surface reconstruction using a surface-from-gradient algorithm, which will allow 3D roughness computation for a later dynamic haptic rendering.

**Results:** Texture and curvature of the 3D reconstructed surface are checked in the first experiment, comparing roughness and geometry errors between a reconstructed surface using the proposed algorithm and two other algorithms, as well with a ground truth surface. The second experiment tests the method using in-vivo real skin disease images to compute roughness estimation and decomposition and also tasting haptic rendering in a haptic device. The experimental results verify the validity of our method.

**Conclusion:** Roughness is a crucial property for dermatologists to examine skin disease (e.g., cases of psoriasis, atopic eczema or aging), that is why the proposed method of roughness estimation for haptic rendering will be extremely useful for dermatologists, improving the skin diagnose. In addition, the proposed method does not require complex medical systems to be implemented, since single image reconstruction is used.

**Key words:**

single image; skin disease images; skin palpation; skin surface reconstruction; 3D roughness; roughness decomposition.

## 1. Introduction

As in any organ, the diagnosis of skin diseases involves various examinations and additional tests occasionally. One of common methods is to rely on visual aspects such as colors and biomechanical surface properties (roughness and dryness). Whilst visual aspects are of great importance in dermatology diagnosis, palpation facilities in determining induration, quality of scaling, and temperature and roughness changes because the visibility on skin may lack objective signs. Even though many studies claim the importance of palpation for dermatologists [1,2], is not always possible to carry out because of the risk of secondary infections or damage to the diseased skin. The goal of this research is to develop a haptic (tactile and kinesthetic) roughness rendering algorithm that enables dermatologists to examine real skin samples without directly palpating infected area of the skin.

Following a similar goal, some years ago was created a prototype of a skin imaging system integrated with haptic feedback device [3] and from a software perspective, some rendering algorithms has been designed to analyze skin surface and roughness [4-6]. Also a new way of 2D haptic roughness measurement was proposed to improve roughness rendering [7]. But it is believed that using 3D roughness estimation instead of 2D is more appropriate for 3D surfaces, since 2D roughness can be restrictive and misleading [8,9]. Hence, in our study is proposed a new direction, computing 3D skin roughness estimation from single image, being the first study that measures roughness including global curvature.

To achieve this, one of the crucial steps is to reconstruct an accurate three-dimensional (3D) skin surface, which forms a geometric structure for haptic rendering with an in-vivo skin image. Despite there are some procedures as 3D laser scanning [10,11] or multi-camera techniques [12,13] that have favorable results in 3D surface reconstruction, they are not optimal for haptic rendering, as their algorithm complexity would preclude instantaneous haptic rendering. That is why previous existing studies for haptic palpation are focused on 3D skin reconstruction from single image [4-7]. Their results are favorable but medical tests are extremely strict in terms of accuracy and reliability and skin surface reconstruction from a single image is truly influenced by image properties (i.e., light conditions, noise), which leads

to a big challenge still in research and improvement.

Trying to reduce the problematic of high influence of image properties in the result, is proposed a new approach based in surface from gradient reconstruction. There are previous successful studies using this method [14-16] but it has never been considered in 3D skin reconstruction for haptic palpation. Furthermore, the proposed approach is based on discrete geometry processing [17], which avoids enforcing integrability constraints that sometimes leads to invalid surfaces due to the perturbed noisy gradients that are non-integrable. The introduced 3D skin roughness reconstruction using a surface-from-gradient algorithm based on discrete geometry processing leads to benefits like sharp feature preservation or possibility to reconstruct surfaces with incomplete data as well as reduction of the noise in the final surface.

Looking back on the goal of 3D roughness rendering algorithm, next crucial step is to introduce the roughness estimation method. In our study the roughness rendering algorithm will compute 3D roughness from the 3D reconstructed surface, obtaining a 3D roughness decomposition that will allow an accurate haptic palpation. Taking advantage of this 3D roughness computation, a way of mapping skin surface roughness decomposition is also introduced, which will be highly useful for skin examination and diagnosis. Since skin disease images are not homogeneous and they have differentiated areas, dermatologists may have regions of interest (ROI), this methodology will add the possibility of evaluating individually different parts of the image, which could be extremely useful to focus more precisely in the area affected area.

To sum up, this study proposes a new direction of 3D skin roughness estimation from single skin image, introducing an accurate 3D skin surface reconstruction using gradient based surface reconstruction. Which will allow a deep roughness analysis highly useful for skin diagnosis. In addition, using the proposed methodology, this study provides new results of 3D skin surface roughness for four skin diseases (acne, miliaria, sweet syndrome and herpes simplex) and for their regions of interest.

In the following sections are explained all the methods proposed to implement the gradient-based skin surface roughness estimation for haptic palpation, along with all the experimental results and discussions. By last, conclusions and future research plan are exposed.

## 2. Material and Methods

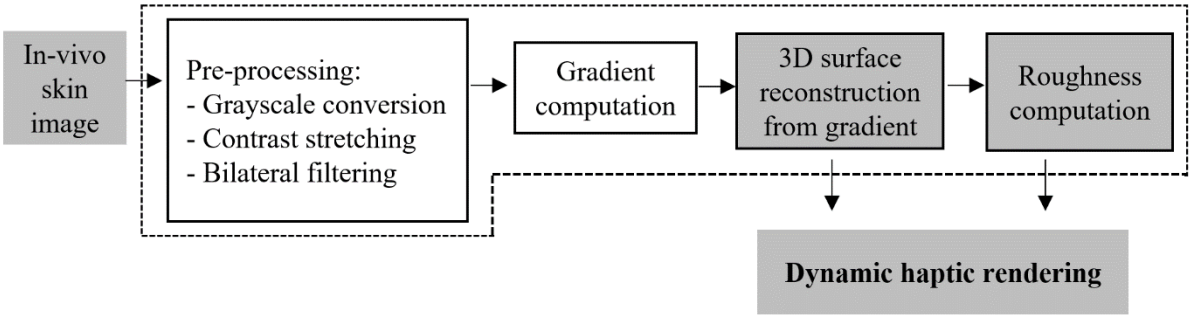


**Fig. 1.** Overview of our proposed approach to 3D roughness estimation and haptic rendering from a single skin image

In this section is described the proposed method, including pre-processing and estimating 3D roughness from a single image for haptic palpation. Fig. 1 shows the block diagram of the methods used to implement it. First step is pre-processing of the 2D image and computation of the gradient, which will be used to reconstruct the 3D surface. By last, 3D roughness computation of the reconstructed surface is done.

### 2.1. Pre-processing of a skin image

In 3D reconstruction from a single image all the information to reconstruct the surface is obtained from the 2D image, that is why the value of the result is strongly influenced by the quality and properties of the image. The way to improve the quality of the 2D image before the 3D reconstruction is pre-process it, which will strongly improve the results, avoiding high frequency noise and improving light conditions that will lead to a more accurate output surface. In our method, the pre-processing includes three steps. First, grayscale conversion is needed to ease image processing. Second, contrast stretching will help to optimize contrast of the image enhancing edges and details differentiation. Ultimately, bilateral filtering will reduce the noise but preserving the edges, to acquire a detailed but smooth surface.

**Contrast stretching**

Contrast stretching is applied to converted gray scale image. This method optimizes the image making use of all the range of intensity values, by using a linear scaling function to map the output pixels values from the inputs. The following equation is used:

$$I_{out} = (I_{in} - c)\left(\frac{b-a}{d-c}\right) + a \quad (1)$$

where $I_{out}$ and $I_{in}$ are the input and output values respectively, a and b are the output limits (for 8-bit grayscale 0-255) and d and c are the limits of the input image.

**Bilateral filtering**

Applying smoothing filters is vital to remove the noise and get an accurate surface reconstruction. There are many smoothing filters like median or gaussian filter, but bilateral filter was chosen because of the importance of edge preserving [18,19]. Filtering an image means compute an output that is function of the input and its neighbors. In the case of gaussian filter the output is calculated as a weighted average of the neighbor values where the weights decrease with the distance. This filter considers only the domain (closeness of the pixels), this is because is assumed that the similarity of pixels value depends on the distance. But this doesn't happen in the edges and consequently are blurred. To solve that, bilateral filter considers not only the domain but also the range (similarity of pixels intensity). In medical image is essential not losing any information of the image because is required an accurate result of the properties, because of that is used a bilateral filter with strong edge-preserving property. To compute the output value of each pixel the image is divided in different regions, determined by the window radio (w), in Fig. 2 is shown an example of one region with domain ($\Omega$). In each region are applied the following equations:

Gaussian kernels:

$$W_{D_{p,q}} = \exp\left(-\frac{1}{2}\frac{\|p-q\|^2}{\sigma_d^2}\right) \quad (2)$$

$$W_R(I_p, I_q) = \exp\left(-\frac{1}{2}\frac{\|I_p-I_q\|^2}{\sigma_r^2}\right) \quad (3)$$

where $p$ is the pixel of interest and $q$ the neighbor pixel. The kernel is applied in the $\Omega$-neighborhood of the pixel $p$. In this case is taken a window radius of 5. The desired amount of domain low-pass filtering is decided by the standard deviation of the spatial-domain ($\sigma_d^2$) and the desired amount of combination of pixels values is decided by the standard deviation of the intensity-domain ($\sigma_r^2$).

In this study, is set the standard desviation of the spatial-domain to 2 and the standard desviation of the intensity domain to 0.15.

Once defined the gaussian weights, the bilateral filter at each point ($B_p$) is defined using the above equations:

$$\emptyset_{p,q}(I_p, I_q) = W_{D_{p,q}} W_R(I_p, I_q) \quad (4)$$

$$B_p = \frac{1}{p}\sum_{q\in\Omega} \emptyset_{p,q}(I_p, I_q) I_q \quad (5)$$

where $W_p$ is the normalizing factor:

$$W_p = \sum_{q\in\Omega} \emptyset_{p,q}(I_p, I_q) \quad (6)$$

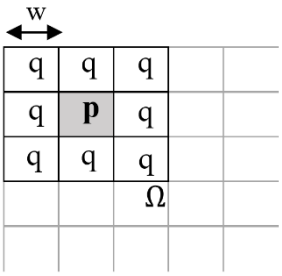


**Fig. 2.** Domain of the image ($\Omega$) defined by the radius window (w).

### 2.2. Gradient computation from a skin image

In this study surface-from-gradient method is used to obtain the 3D surface, hence there is a need to

compute the gradient field of the image. The gradient is a measure of the pixels intensity change. The modulus depends on the intensity magnitude and the direction points to the direction of greatest increase. In 2D domain the gradient can be defines as the partial derivative of the intensity in $x$ and $y$ direction:

$$\nabla I = [I_x, I_y] = \left[\frac{\delta I}{\delta x}, \frac{\delta I}{\delta y}\right] \quad (7)$$

For discrete data can be approximated using finite differences:

$$\frac{\delta I(x,y)}{\delta x} \approx F(x+1, y) - F(x, y) \quad (8)$$

$$\frac{\delta I(x,y)}{\delta x} \approx F(x+1, y) - F(x, y) \quad (9)$$

To compute the equations for an image, is used matrix based numerical differentiation and it is required a kernel to effectively compute the discrete derivative values. In our case is used the Sobel operator to approximate the derivatives. This operator uses the below 3x3 kernel:

$$I_x = \begin{pmatrix} -1 & 0 & 1 \\ -2 & 0 & 2 \\ -1 & 0 & 1 \end{pmatrix} \quad (10)$$

$$I_y = \begin{pmatrix} -1 & -2 & 1 \\ 0 & 0 & 0 \\ -1 & 2 & 1 \end{pmatrix} \quad (11)$$

The main characteristic of this operator is to emphasize with factor 2 the points in the same row or column, $x$ and $y$ derivatives respectively.

### 2.3. 3D skin surface reconstruction from skin image gradients

As revealed before, a surface-from-gradients algorithm will be used. There are many studies using this technique. Most of them solve a continuous reconstruction problem via last-square-optimization [14,15] but the algorithm used transfer the continuous problem to a discrete geometry problem solved via last-square-optimization [17]. Working in the discrete domain avoids enforcing integrability constraints to the perturbed non-integrable gradient that sometimes can provoke invalid surfaces. The method is divided in two steps; local blending, where the facets of the surface are oriented individually and global blending, where the facets are glued to obtain the reconstructed surface. These two steps are explained in detail

below. This algorithm introduces some advantages that will be useful in skin reconstruction. One of them is the preservation of sharp-feature, as the normal vectors are only enforced inside facets and there is not integrability constraints enforced in all the surface, that will help to avoid distortion and preserve important details even with sharp features. Another advantage is the possibility to reconstruct the surface with missing data, it is demonstrated that this method has good results for sparse gradient fields, it will help to obtain good results for example when the image is perturbed with light reflection (white pixels appear) or when there is salt and pepper noise. By last, the global blending will help to reduce the noise obtaining a smooth surface. Our goal is to take advantage of this method in the study of real skin surface reconstruction. The details for solving the reconstruction problem are explained below.

The input needed is an image gradient $\nabla I$. It is a vector formed for a set of 2D points, that define the gradient at each image pixel. To solve the problem in the discrete domain, one facet $f_{x,y}$ is defined for each sample $(x, y)$. The normal vector of this facet will be constructed from the input gradients following the next equation:

$$n = \frac{(-g_x, -g_y, 1)}{\sqrt{g_x^2 + g_y^2 + 1}} \quad (12)$$

Each facet contains 4 vertices that are defined as:

$$v_{x,y} = \left(\left(x - \frac{1}{2}\right)h,\ \left(y - \frac{1}{2}\right)h, 0\right) \quad (13)$$

where $h$ is the pixel width. The z value starts in 0, which implies a planar surface $S$ defined by the facets $f_{x,y}$ and vertices $v_{x,y}$.

To find the final surface $S$ is needed to solve an optimization problem. The optimal case will be to enforce the normal vector of $S$ equal to the normal vector of each facet $f_{x,y}$, $n_{x,y} = n(f_{x,y})$, but this is too restrictive and will lead to large computation, hence, this algorithm is solved with a weaker constraint, both normal vectors should be parallel $n_{x,y} \parallel n(f_{x,y})$.

The algorithm is divided in two steps, local blending and global solution

**Local shaping**

In this step every facet $f_{x,y}$ should be oriented to agree the normal vector $n_{x,y}$. To get this, every vertex $v_{x,y}$ is projected to the desired plane, maintaining $x$ and $y$ values and changing $z$, as is shown in Fig. 3.

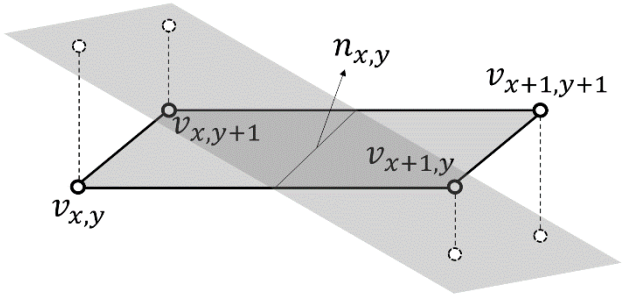


**Fig. 3**. The figure shows the projection of the vertex in the desired plane

The vertices that are contained in 4 facets, will obtain 4 projected positions. The ideal case is $n_{x,y} = n(f_{x,y})$, where all the positions would be equal, but this doesn't happen in the reality and the result are independent oriented faces that should be glued through optimization process to finally obtain the continuous surface $S$ .

**Global blending**

The goal of the global blending is to construct the final surface $S$. To do that it is necessary to find the z values for each vertex. To solve the problem two vectors are defined:

$$p(f_{x,y}) = [\, d_{x,y} \;\; d_{x+1,y} \; d_{x+1,y+1} \;\; d_{x,y+1} \;]^T \quad (14)$$

$$q(f_{x,y}) = [\, h_{x,y} \;\; h_{x+1,y} \; h_{x+1,y+1} \;\; h_{x,y+1} \;]^T \quad (15)$$

$p(f_{x,y})$ contains the $z$ values obtained projecting the vertex in the local shaping ($d_{x,y}$) and $q(f_{x,y})$ is the vector with the output $z$ values ($h_{x,y}$).

The goal is finding a functional to minimize in the optimization process. The ideal case is $p(f_{x,y}) = q(f_{x,y})$, so we could use the difference between these two vectors as functional, but it is too restrictive, and it is assumed that the $z$ position can vary but the facets $f_{x,y}$ will preserve the shape. To assure that are computed the relative vectors with reference to their own center, defined as $Md(f_{x,y})$

and $Mp(f_{x,y})$ and finally the functional to minimize will be the following:

$$\phi(z_{k,l}) = \sum_{f_{x,y}} \left\| Md(f_{x,y}) - p(f_{x,y}) \right\|^2 \quad (16)$$

### 2.4. 3D roughness estimation

This study introduces a 3D roughness estimation from 2D skin image gradients, estimating roughness from the 3D reconstructed surface. The algorithm used estimates pixel roughness from the 3D surface. This algorithm measures the local roughness derived from Gaussian curvature [20,21]. Gaussian curvature provides an idea of how differ the mesh in the vertex neighborhood from a planar surface, accordingly, in a planar surface the gaussian curvature will be null. The discrete Gaussian curvature in each vertex ($K_{g_i}$) is estimated by the method named *angle deficit:*

$$K_{g_i} = \left| 2\pi - \sum_{j=1}^{N} \alpha_j \right| \quad (17)$$

where $\alpha_j$ is the angle at $v_i$ formed by the $j$-th facet and N are all the neighbor facets. In Fig. 4. is shown a vertex $v_i$ and the angles $\alpha_j$ formed by its 6 neighbor facets (N=6).

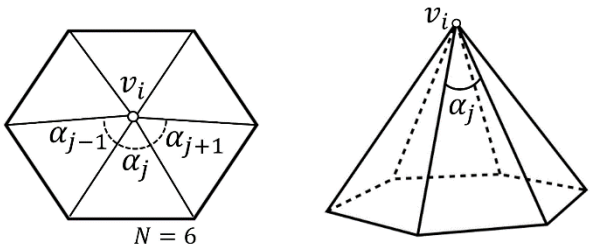


**Fig. 4**. Application of *angle deficit* method for computing the discrete Gaussian curvature. Triangles embedded in 3D (left) and 3D geometry (right).

Local roughness at each point ($R_i$) is computed as the Laplacian of the discrete Gaussian curvature. Using the Laplacian of the curvature instead of the gaussian curvature by itself involves more vertices and facets in the computation so provides a more robust result [22]. Moreover, this method computes the difference of curvatures which avoid confusing a high curvature smooth surface with a rough surface. The local roughness is evaluated as a weighted difference of the discrete gaussian curvature at each

vertex $v_i$ and its $v_j$ neighbors. In Fig. 5. is shown a vertex $v_i$ and its neighbors $v_j$ as well as the angles $\theta_{ij}$ and $\beta_{ij}$ needed to compute the roughness.t

$$R_i = \sum_{j \in N(i)} w_{ij}(K_{g_i} - K_{g_j}) \quad (18)$$

The weights are determined by the cotangents:

$$R_i = \sum_{j \in N(i)} \frac{1}{2}(cot\theta_{ij} + cot\beta_{ij})(K_{g_i} - K_{g_j}) \quad (19)$$

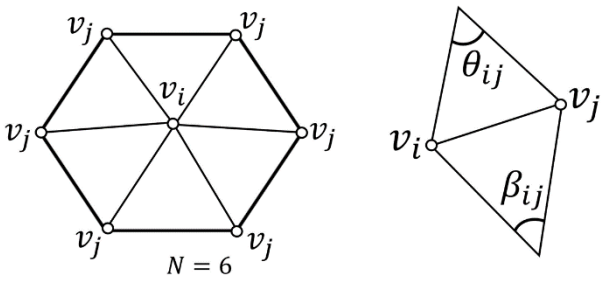


**Fig. 5.** vertex $v_i$ and its neighbors (left). Angled used for the cotangent weights.

The roughness computed at each point can be mapped, obtaining a roughness decomposition map of the 3D mesh. For each surface can be also computed the roughness mean and variance. As the mean of the roughness at each vertex and its variance.

## 3. Results

The goal of the study was to propose a truthful haptic roughness estimation and rendering, since as above-mentioned it is crucial for a successful skin disease diagnose. To get this, was developed an algorithm that estimates 3D roughness from a 2D single image that can be taken with an electronic microscope. The roughness estimation is computed from the 3D skin surface reconstruction. That is why the first important step is to have an accurate reconstructed surface. Surfaces has two important characteristics; global curvature, that gives information about the geometry of the surface and local texture, that shows the wrinkles and rugosity of the skin. The viability in in terms of both roughness and curvature, are checked in the first experiment (experiment I), comparing the proposed method with other existing methods and with a ground truth.

The goal of the second experiment (experiment II) was to verify the method in a realistic case. Roughness estimation and haptic rendering for in-vivo skin disease images was done to prove the proposed approach with real skin disease images. These two experiments are explained in detail in this section. In this study is used a computer (Intel i7-770 @ 3.60 GHz, RAM 32 GB, NVIDIA GeForce GTX 1050). In all the experiment the algorithms were implemented using Matlab 2016a.

**Experiment I: verification of 3D surface reconstruction**

The goal of this experiment was to validate the 3D surface reconstruction. Surfaces has two important characteristics; global curvature, that gives information about the geometry of the surface and local texture, that shows the wrinkles and rugosity of the skin. In this study to prove the 3D surface were verified both texture and curvature.

To perform the experiment were needed two plaster hands, obtained with a water-based skin-safe molding powder to cast hand molds. This plaster hands were scanned using a 3D professional scanner (Capture Scanner, 3D Systems, Resolution: 0.110 mm at 300 mm or 0.180 mm at 480 mm) and software (Geomagic, 3D Systems), the process is shown in Fig. 7. Likewise using the software Geomagic, were extracted 6 surfaces from the two models to use as ground truth (GT), the surfaces are exposed in Fig. 8. 2D images of the ground truth surfaces were captured to use as 2D single image input to test the algorithms, Fig. 9 contains the images.

To verify the roughness the proposed 3D roughness estimation method from the surfaces was used. Regarding to geometry errors a methodology using Hausdorff distance was introduced, using the software (MeshLab 2016.12). First step was to rescale the models to have the same scale. After that a finite iterative closest point algorithm that uses finite difference optimization was used to compute the transformation matrix to move one of the models to overlap the meshes. Once the meshes were in the minimum error position, Hausdorff distance was computed between them.

Using the 6 ground truth surfaces and the 6 2D image the comparison process explained below and exposed in Fig. 6 was repeated 6 times, one for each surface:

1) Obtention of three reconstructed surfaces using the 2D image as input and using the proposed algorithm and two other algorithms (A1 and A2).

2) Computation of 3D roughness using our proposed method.

2.1) Roughness estimation ($R_{est}$) for the ground truth surface and for the reconstructed surfaces. And computation of roughness error, as the difference between the ground truth surface value and the reconstructed surfaces value. Results shown in Table 1.

2.2) Processing of the roughness map decomposition for the ground truth surface and for the reconstructed surfaces. Shown in Figs.10 and 11.

3) Computation of geometry errors using the methodology exposed above.

3.1) Calculation of the Hausdorff distance between the ground truth surface and the reconstructed surfaces. Results shown in Table 1.

3.2 ) Processing of the Hausdorff distance map for the reconstructed surfaces. Shown in Fig. 12

4) Visual examination to compare the reconstructed surfaces, exposed in Fig. 9 and the GT surfaces, exposed in Fig. 8.

The reconstruction should be validated in two ways, noticing the similarity of the reconstructed surface by the proposed method and the ground truth surface and confirming that the reconstructed surface using the proposed algorithm has better result than the surfaces reconstructed using the other algorithms.

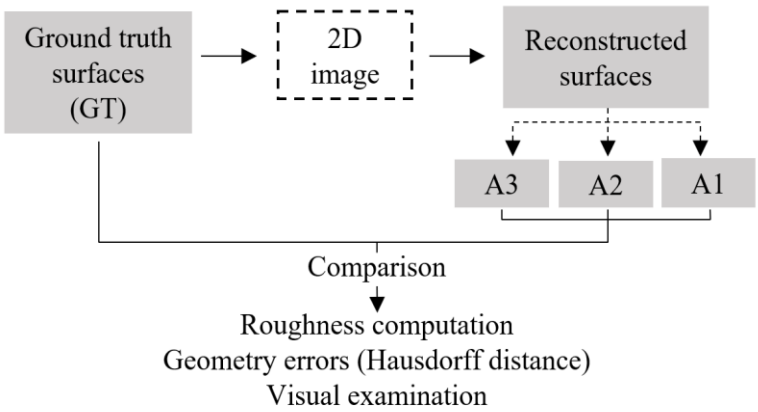


**Fig. 6.** Scheme of the experiment I. This comparison methodology will be applied for the 6 surfaces

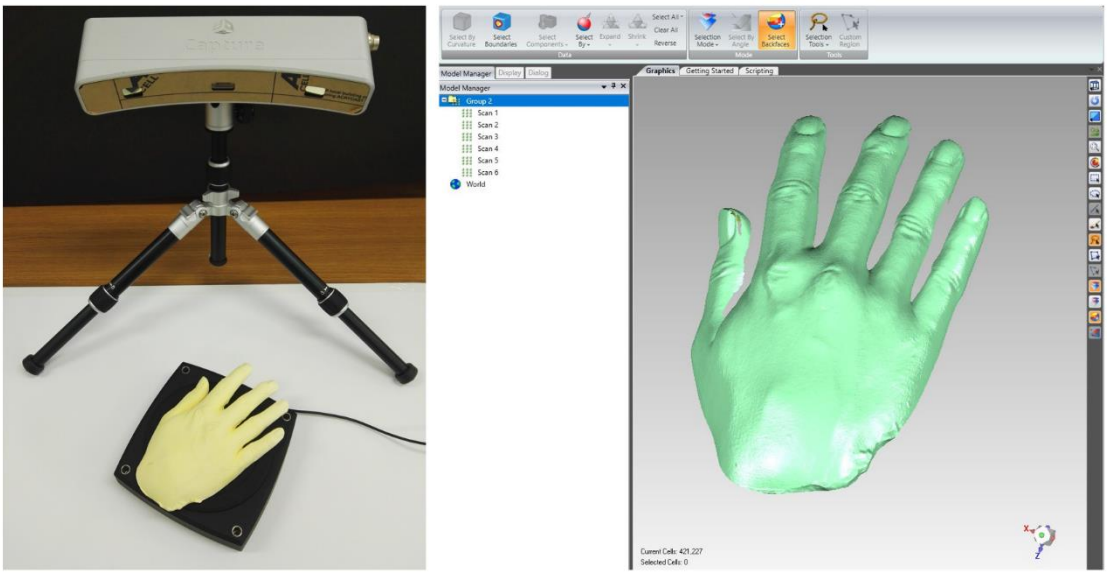

**Fig. 7.** (Left) 3D Systems Capture scanner scanning one of the skin stone models. (Right) Geomagic software obtaining the scanned model

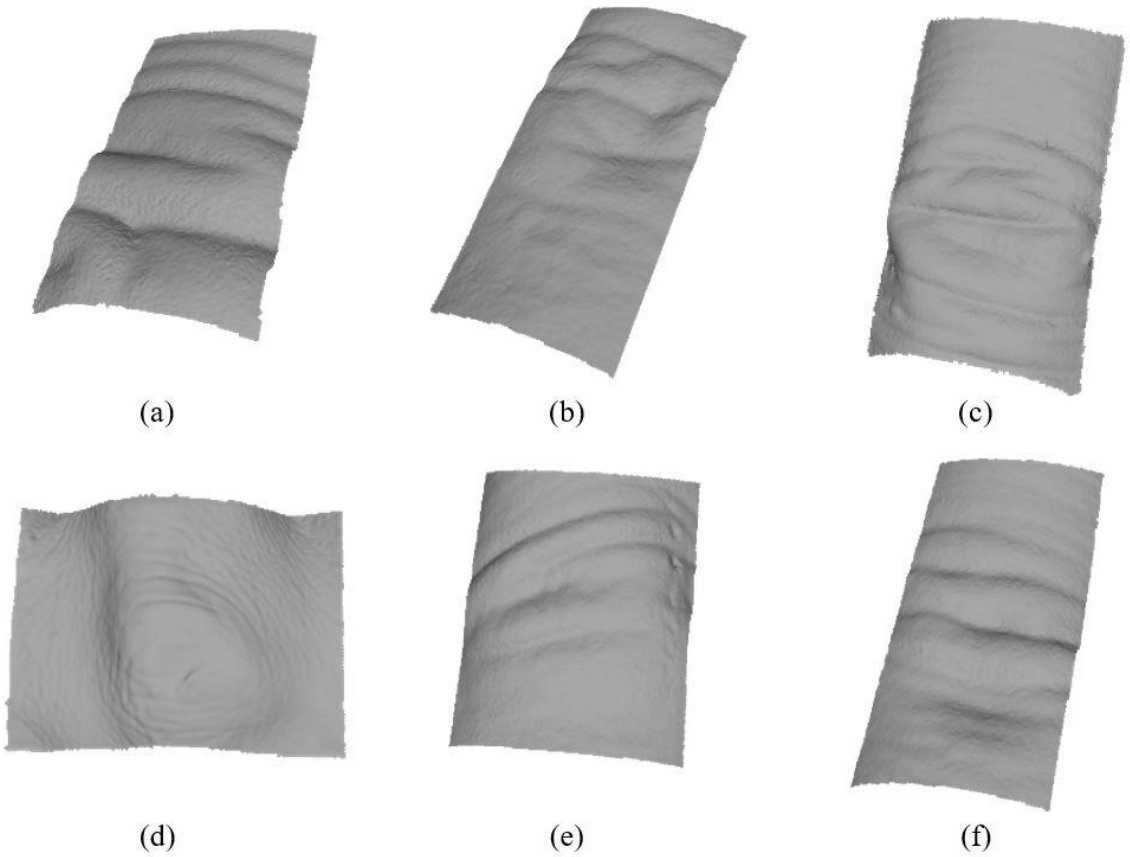


**Fig. 8.** Ground truth surfaces (GT) extracted from the 3D scanned models. (a) Surface 1 (SS1), (b) Surface 2 (SS2), (c) Surface 3 (SS3), (d) Surface 4 (SS4), (e) Surface 5 (SS5), (f) Surface 6 (SS6)

**Table 1.** Accuracy of 3D surface reconstruction. Our results are compared with other methods (A1 and A2) in terms of $R_{est}$ (Roughness estimation), $R_{err}$ (Absolute error in roughness) and RMS (Root mean square)

| | Our method | | | A1 | | | A2 | | |
|---|---|---|---|---|---|---|---|---|---|
| | $R_{est}$ | $R_{err}$ | RMS | $R_{est}$ | $R_{err}$ | RMS | $R_{est}$ | $R_{err}$ | RMS |
| SS1 $R_{est}$ of GT: 0.01151 ±0.00036 | 0.00846 ±0.00044 | 0.00305 | 0.02088 | 0.14106 ±0.02246 | 0.12955 | 0.02299 | 0.02994 ±0.00152 | 0.01843 | 0.02345 |
| SS2 $R_{est}$ of GT: 0.00492 ±0.00006 | 0.0082 ±0.0004 | 0.00328 | 0.01746 | 0.12175 ±0.01576 | 0.11683 | 0.02001 | 0.02299 ±0.00088 | 0.01807 | 0.02071 |
| SS3 $R_{est}$ of GT: 0.00391 ±0.00056 | 0.00306 ±0.00025 | 0.00084 | 0.02927 | 0.1264 ±0.01742 | 0.12249 | 0.03389 | 0.02353 ±0.00101 | 0.01962 | 0.03361 |
| SS4 $R_{est}$ of GT: 0.00156 ±0.00044 | 0.00653 ±0.0003 | 0.00497 | 0.07585 | 0.11778 ±0.01497 | 0.11622 | 0.07942 | 0.0236 ±0.00094 | 0.02204 | 0.07939 |
| SS5 $R_{est}$ of GT: 0.00549 ±0.00017 | 0.00305 ±0.00028 | 0.00244 | 0.03349 | 0.12295 ±0.01633 | 0.11746 | 0.04023 | 0.02419 ±0.00101 | 0.01870 | 0.03964 |
| SS6 $R_{est}$ of GT: 0.00456 ±0.00006 | 0.1194 ±0.01516 | 0.11484 | 0.02723 | 0.1194 ±0.01516 | 0.11484 | 0.02723 | 0.02216 ±0.00084 | 0.01760 | 0.02782 |

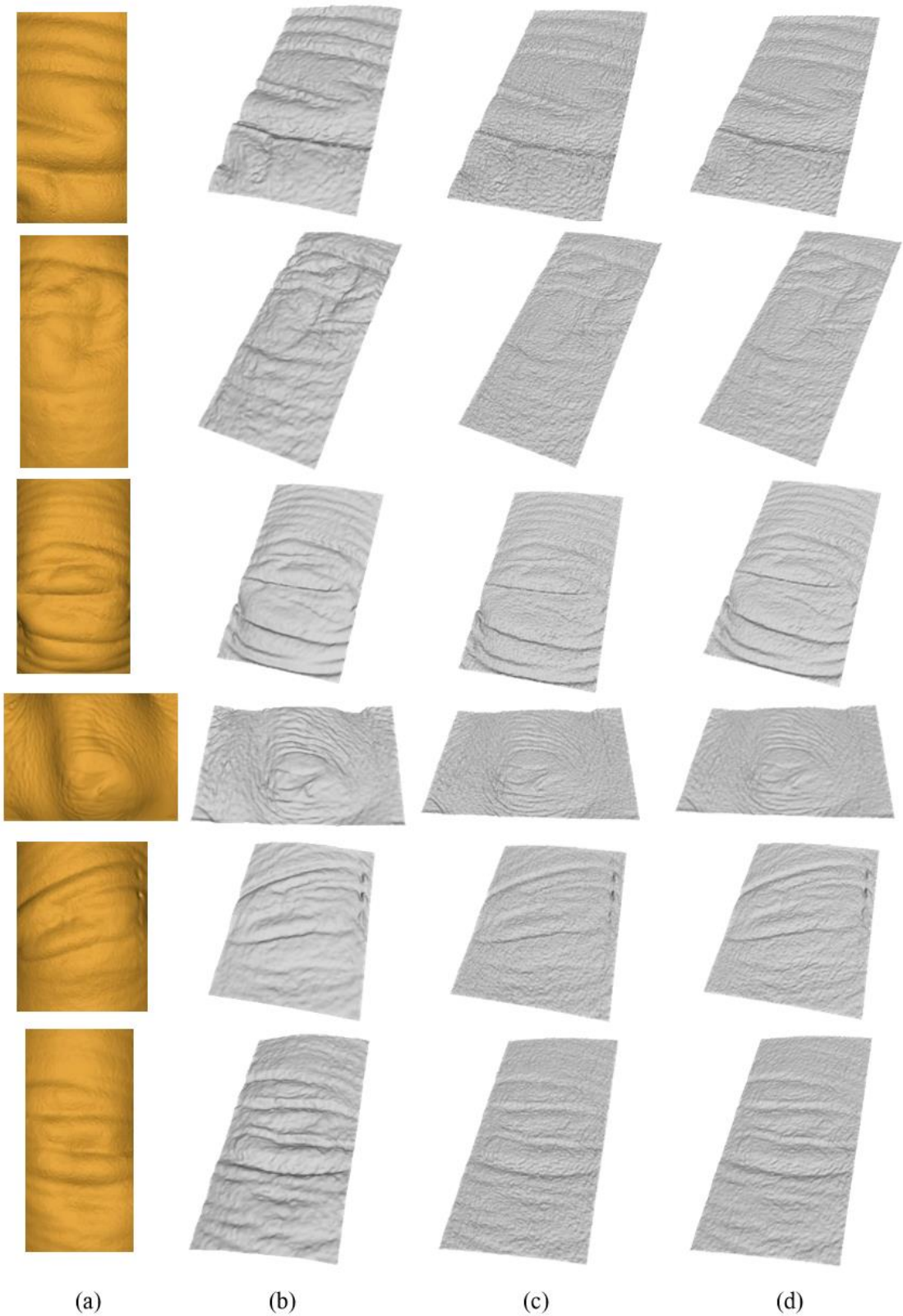


**Fig. 9.** Resulting images of 3D skin surface reconstruction comparing with other methods (A1 and A2). Images in column (a) are 2D images, SS1 (339x674), SS2 (322x687), SS3 (367x627). (d) SS4 (572x422). (e) SS5 (393x510). (f) SS6 (326x667). (b) are results of our proposed method, (c) and (d) results of A1 and A2 respectively.

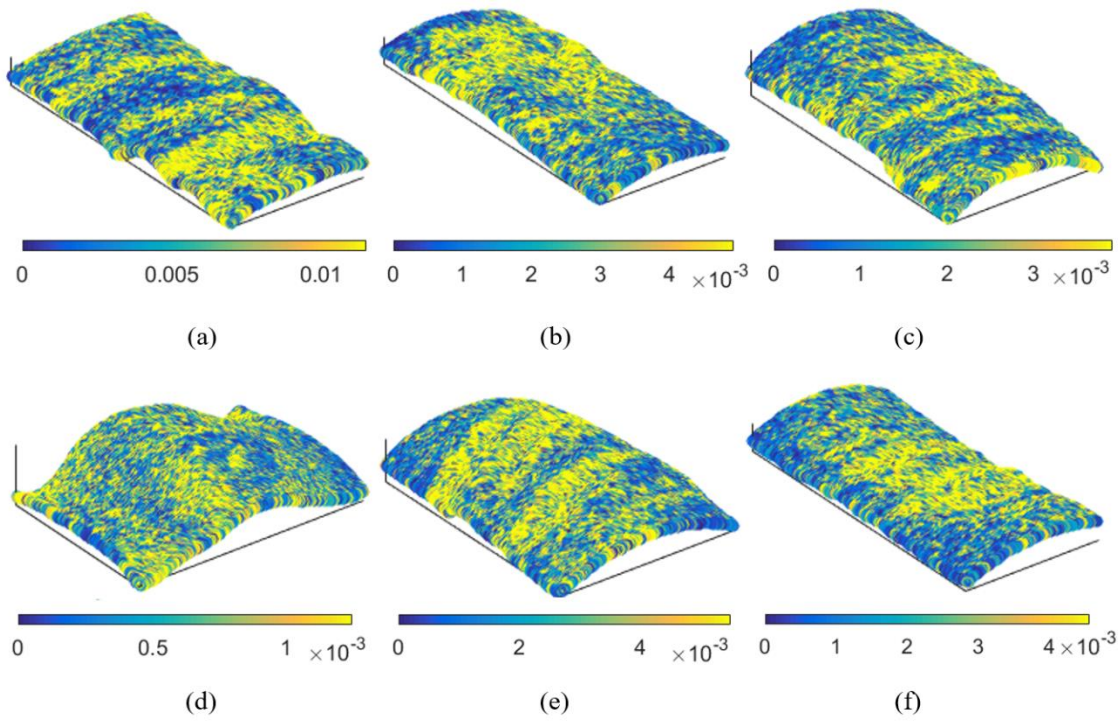


**Fig. 10.** Roughness decomposition of the ground truth surfaces. (a) SS1, (b) SS2, (c) SS3, (d) SS4, (e) SS5, (f) SS6.

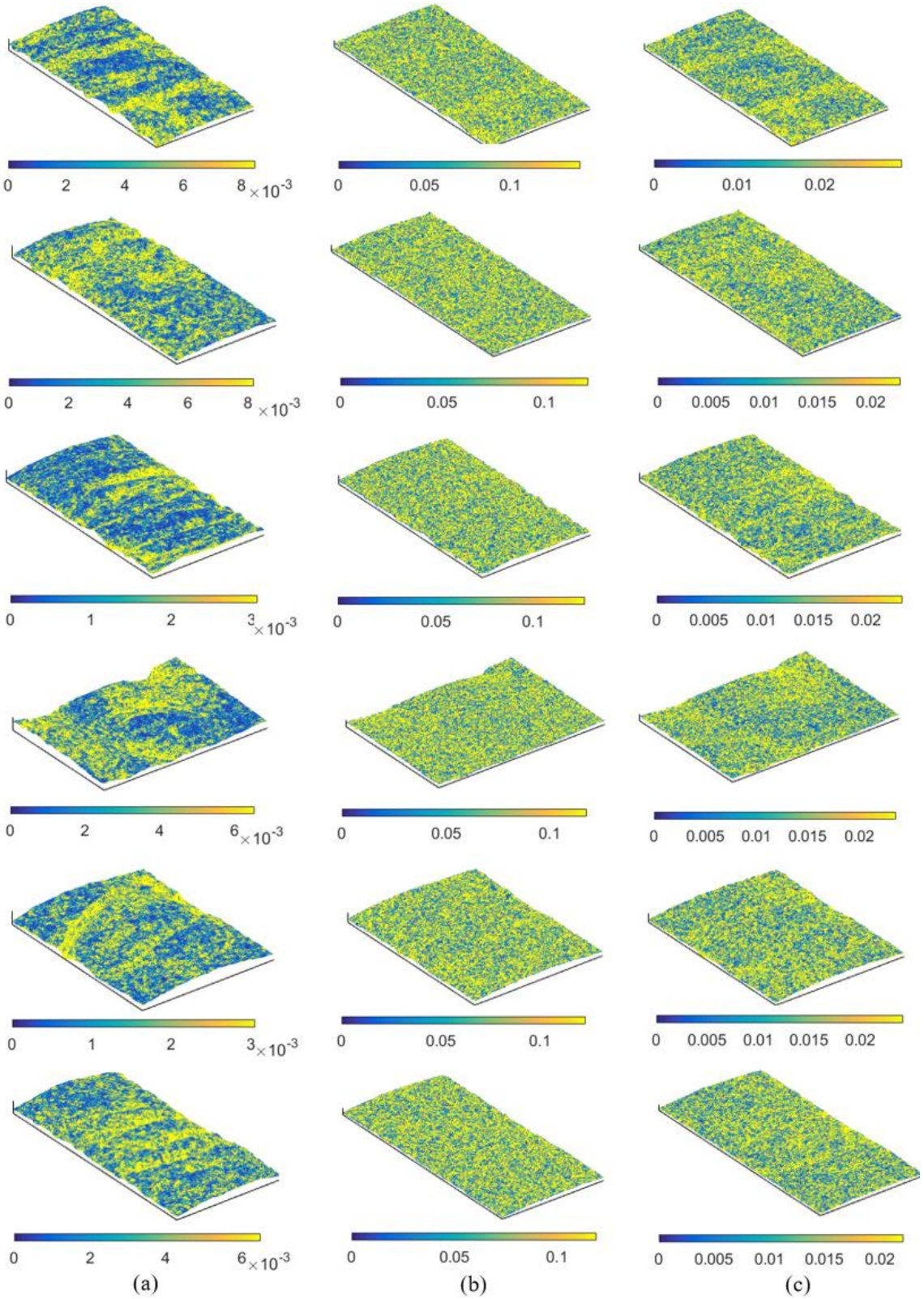


**Fig. 11.** Roughness decomposition of the reconstructed surfaces. Column (a) results of our proposed method, (b) and (c) results of A1 and A2 respectively.

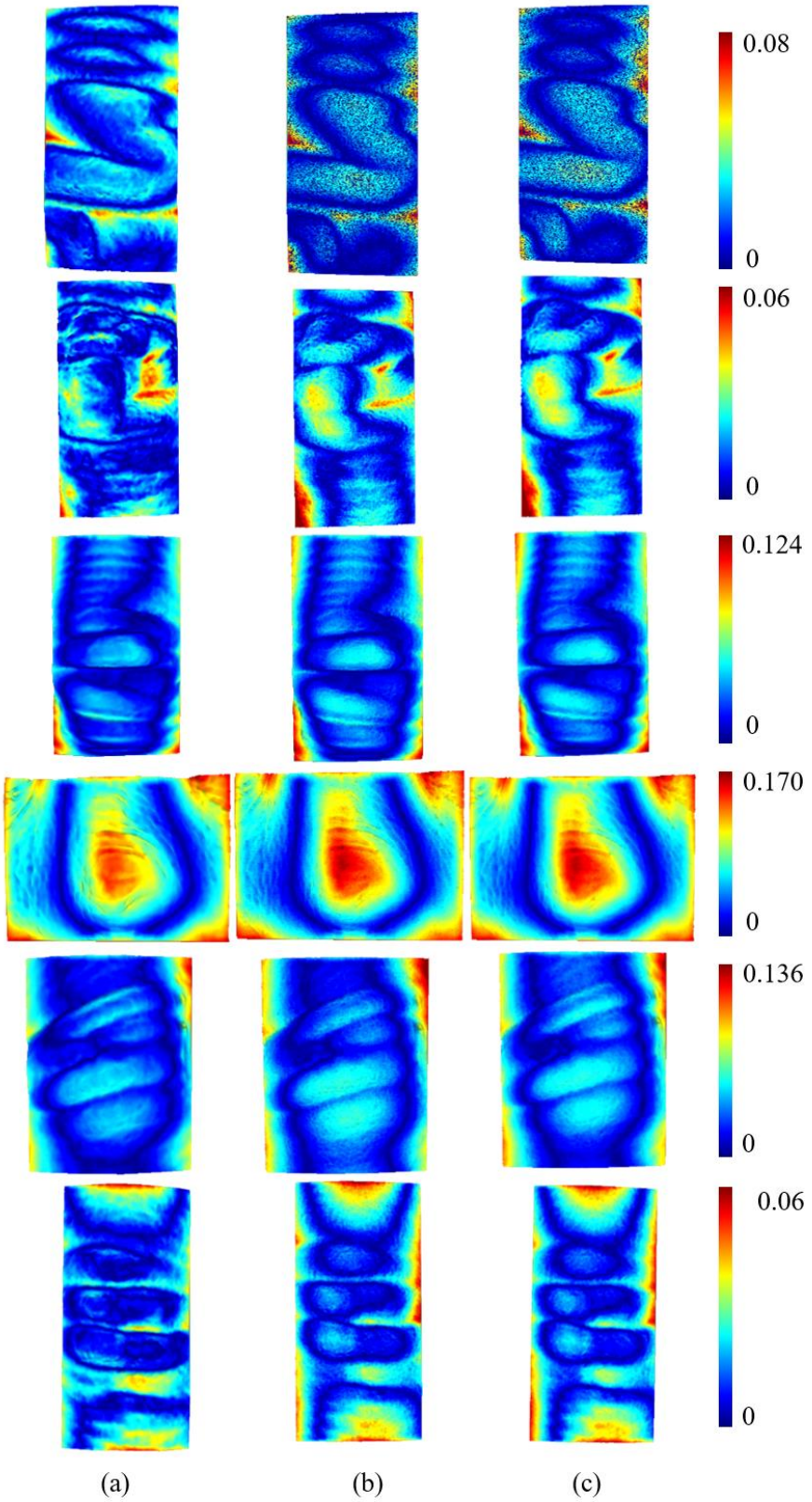


**Fig. 12.** Geometry error map of the Hausdorff distance. In (a) between GT and resulting surface of our proposed method, (b) and (c) between GT and A1 and A2, respectively.

**Experiment II: 3D roughness estimation with in-vivo skin disease images and haptic rendering**

The goal of this experiment is to prove the proposed approach for real skin disease. To perform the experiment 4 in-vivo real skin disease images were used as input (see Fig. 13).

In this experiment are implemented all the steps of the methodology, Fig. 1. From the skin disease images are computed the gradients to reconstruct the surface using the proposed surface-from-gradients algorithm. In Fig. 14. are shown the reconstructed surfaces and it is manifest their validity.

It is observable that the skin diseases images have different regions, they are not homogeneous in all the domain, there are health areas as well as areas where the disease appear with different intensities (i.e., in Fig. 13 (a) the disease appears only in the middle), that is why the dermatologists may have regions of interest (ROI). The roughness study is done in both, complete image and ROI. In Table 2. are shown the results of roughness mean and variance and in Fig. 15 are shown the 3D roughness maps. The possibility to decompose roughness and choose the region of interest is a big advantage for dermatologists, since will improve highly the level of detail, enabling the examination of different regions in the same image.

By last, to finish the methodology the results was carried out the dynamic haptic rendering, using the methodology of rendering for haptic palpation exposed in [3] and the haptic device with 3 degrees of freedom (3DOF), Geomagic Touch X. The system is shown in Fig.16.

(a) (b) (c) (d)

**Fig. 13.** In-vivo skin disease images for roughness estimation. (a) Skin Disease 1 (SD1): herpes simplex (300x300). (b) Skin Disease 2 (SD2): miliaria (300x268). (c) Skin Disease 3 (SD3): sweet syndrome (300x300). (d) Skin Disease 4 (SD4): acne (300x300). All images are real

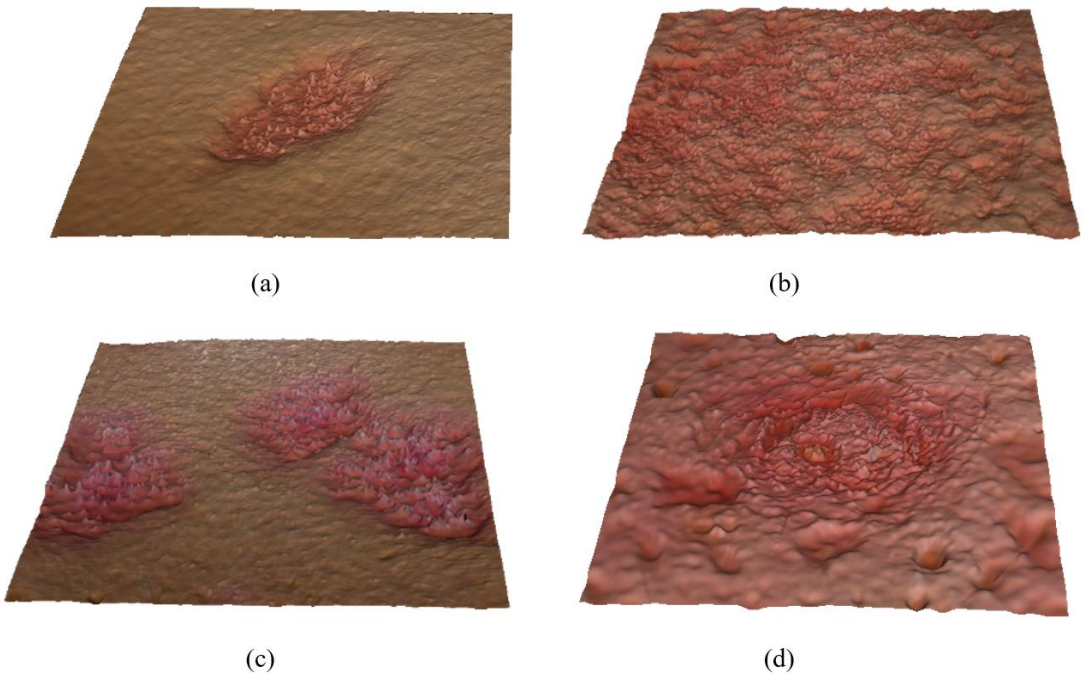


**Fig. 14.** Reconstructed 3D skin surfaces from 2D single images shown in Fig. 13

**Table 2.** Skin surface roughness of the complete real skin diseases images and of the region of interest (ROI)

| ID | Condition | Roughness | | Roughness (ROI) | |
|---|---|---|---|---|---|
| | | Mean | Variance | Mean | Variance |
| SD1 | herpes simplex | 0.00995 | 0.00003 | 0.03947 | 0.00023 |
| SD2 | miliaria | 0.06214 | 0.00009 | 0.08830 | 0.00009 |
| SD3 | sweet syndrome | 0.04219 | 0.00014 | 0.07194 | 0.00041 |
| SD4 | acne | 0.01066 | 0.00001 | 0.03365 | 0.00008 |

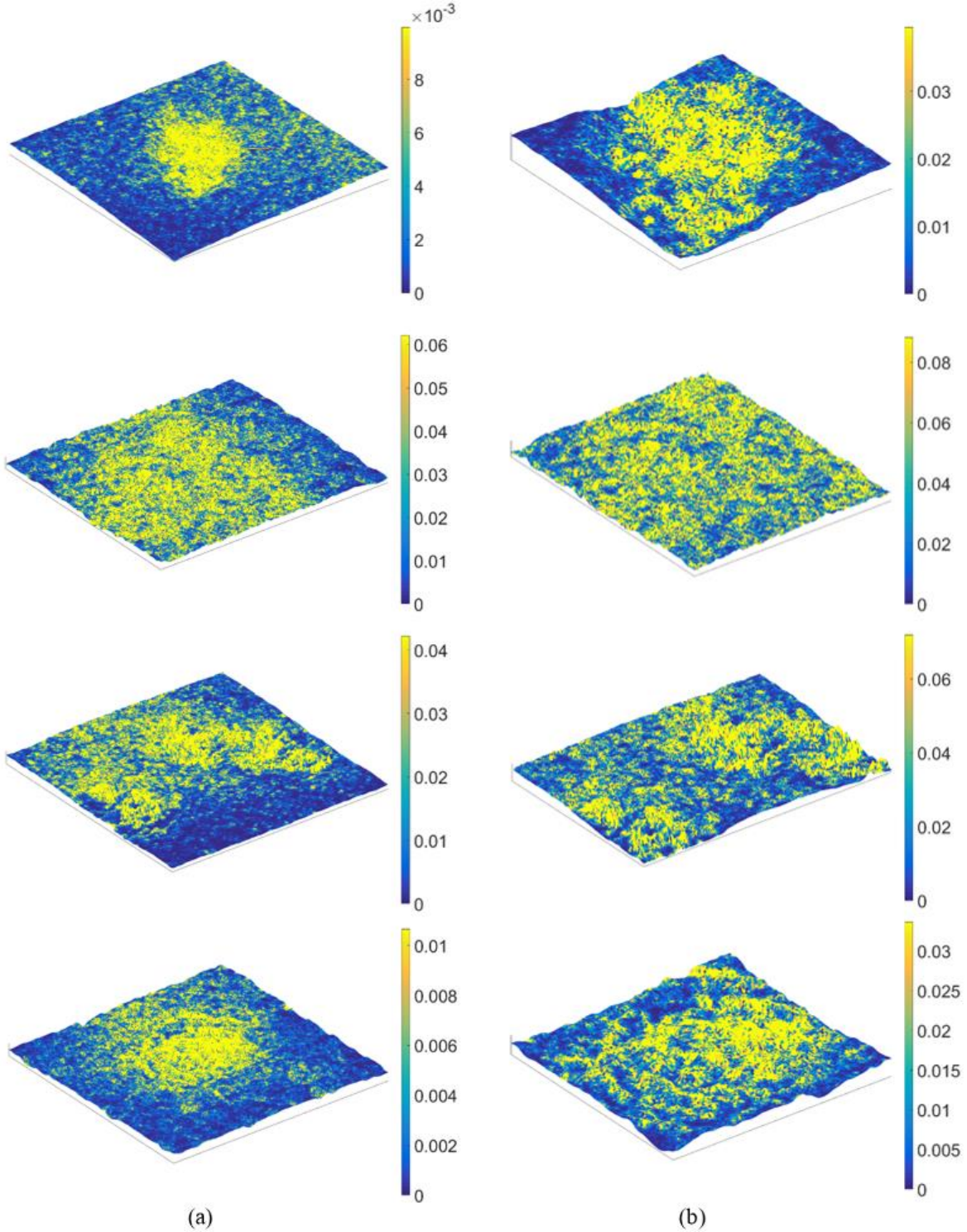


**Fig. 15.** Roughness decomposition of the reconstructed 3D surfaces of the skin disease images corresponding to the reconstructed surfaces in Fig.13. Column (a) complete image and column (b) region of interest (ROI).

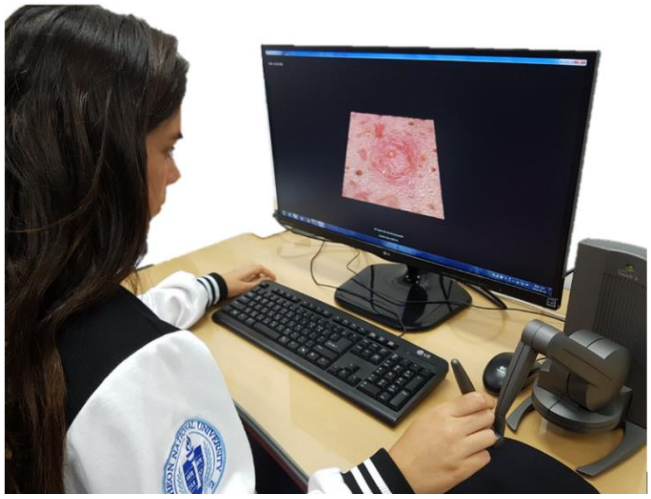

**Fig. 16.** Roughness decomposition of the reconstructed 3D surfaces of the skin disease images corresponding to the reconstructed surfaces in Fig.13. Column (a) complete image and column (b) region of interest (ROI).

## 4. Discussion

The results of experiment I and II, show the viability of the proposed approach, checking the methodology in both, experimental (experiment I) and real case (experiment II).

Watching at Fig. 9 it is possible to make a first visual examination of the reconstructed surfaces. It is visually remarkable that the proposed method has a better reconstruction than algorithms A1 and A2, and the numerical results that will be analyzed below confirm it.

In reference to roughness, in Fig 10 are shown the roughness decomposition maps of the GT surfaces, it is clearly distinguishable areas with different levels of roughness, forming a heterogeneous pattern. In Fig. 11 are shown the roughness maps of the reconstructed surfaces, it is evident that results for algorithm A1 and A2 are not good, because of the high frequency noise, the roughness decomposition map is really confusing, and it is difficult to differentiate a distribution, they seem to have a homogeneous roughness pattern. Even if A2 seems to have slightly better results than A1, they are far worse than the results of our proposed method. The roughness decomposition map of our proposed method (Fig. 10 column (a)) demonstrate that the results are fairly better than for A1 and A2, showing a similar pattern as in the GT map.

About the roughness numerical results exposed in Table 1, it is also noticeable that A1 and A2 are far

from the GT results, having high error. This is because the high frequency noise drive to overly really high roughness. The proposed algorithm has favorable numerical results. Going more deeply, the results are better for smoother surfaces as SS3 and SS4, their roughness mean is a bit smaller and the roughness error too. In the same way, SS6 has the biggest mean roughness and error. This is because of the difficulty to reproduce an accurate roughness, so for rough surface there is more distortion.

About geometry error, it is computed as the Hausdorff distance. In our results it is visible (Fig. 9) that the reconstructed surfaces have highly similar pattern as the ground truth. The numerical results about the curvature are better in our proposed method but not as far as the other two algorithms (A1 and A2) as in the roughness case. The geometry error increases for high curvature surfaces, it is evidenced seeing in Table 1 that SS4 has the biggest error, since has really big curvature and the flatter one, SS6, has the minimum. This is because it is a challenging problem to reconstruct a good curvature from a single image, since there is a lack of depth information.

In the experiment II, roughness estimation and decomposition were done for four skin disease (acne, miliaria, sweet syndrome and herpes simplex). With this experiment it is proved the viability of applying this method in real cases, since the experiment was done from in-vivo real skin disease image through dynamic haptic rendering. The reconstructed surface has satisfactory results, as well as the roughness computation and mapping. In roughness numerical results is noticeable that they change when are computed for the region of interest, in specific in ROI the roughness is higher compared with the roughness of the complete image, SS1 has the biggest change of roughness, since the ROI is a small region in the middle and in the complete image roughness results are distorted by the smoothness of its around. This is a prove of the usability for dermatologists, who can obtain more accurate results of the disease, avoiding not interesting regions. The region of interest can be chosen by visual examination of the dermatologist or by thresholding the roughness value, since it is obvious (Fig. 15) that the different regions are clearly distinguishable by different roughness. By last, the dynamic haptic rendering was successfully carried out, in Fig. 16. is shown the system used, which is the final corroboration of the methodology.

## 5. Conclusions

In this paper is proposed a new geometrical approach for 3D haptic roughness rendering from skin image gradients towards haptic palpation. We developed a methodology that introduce an accurate 3D surface reconstruction from image gradient field that will allow 3D roughness estimation and decomposition, this will provide dermatologists with the possibility of analyzing skin roughness in a precise way, choosing the region of interest for them as well as of a realistic palpation of the skin surface.

Because of the extremely importance of roughness for skin disease diagnose and evaluation, the proposed methodology will be highly useful for dermatologists. Furthermore, the algorithm proposed is simple and efficient, this will lead to advantages like real-time rendering and the need or low-cost system required. It would be extremely easy to implement it in hospitals, without need of new skills or medical systems.

The main challenge relapse in improve the 3D surface reconstruction, the strictness that medical tests entail, makes 3D reconstruction from a single image a difficult goal to achieve. That is why it is still needed research and work to get accurate results and reduce the probability of error. Although the proposed algorithm has good results in many cases, there are some situations that still lack of optimization. Examples of complicated and challenging cases are images that contains many changes of color tonality or images with light reflecting problems. For future studies it would be interesting considering introduce machine learning, since this could be a solution to optimize some problematic cases in which the algorithm needs more information than pixel values to be able to differentiate the situation.

Another way to get improvements could be a new approach for gradient computation, since the reconstructed surface use image gradients will be truly useful an improvement int his technique.

## References


1. Punj P, Devitt PG, Coventry BJ, Whitfield RJ. Palpation as a useful diagnostic tool for skin lesions. *Journal of Plastic, Reconstructive & Aesthetic Surgery.* 2014;67(6):804-807.
2. Cox N. Palpation of the skin--an important issue. *Journal of the Royal Society of Medicine.* 2006;99(12):598.
3. Lee O, Lee K, Oh C, Kim K, Kim M. Prototype tactile feedback system for examination by skin touch. *Skin Research and Technology.* 2014;3(20):307-314.
4. Kim K. Roughness based perceptual analysis towards digital skin imaging system with haptic feedback. *Skin Research and Technology.* 2016;22(3):334-340.
5. Kim K, Lee S. Perception-based 3D tactile rendering from a single image for human skin examinations by dynamic touch. *Skin Research and Technology.* 2015;21(2):164-174.
6. Lee K, Kim M, Kim K. 3D skin surface reconstruction from a single image by merging global curvature and local texture using the guided filtering for 3D haptic palpation. *Skin Research and Technology.* 2018.
7. Kim K. Image-based haptic roughness estimation and rendering for haptic palpation from in vivo skin image. *Medical & biological engineering & computing.* 2018;56(3):413-420.
8. Ramasawmy H. Comparison between 2D And 3D Surface Roughness Parameters for EDM Surfaces. *University of Mauritius Research Journal.* 2001;7.
9. Deleanu L, Georgescu C, Suciu C. A comparison between 2D and 3D surface parameters for evaluating the quality of surfaces. Paper presented at: 3rd International Conference on Diagnosis and Prediction in Mechanical Systems Engineering; 31 May-1 June, 2012; Galati, Romania.
10. Kuş A. Implementation of 3D optical scanning technology for automotive applications. *Sensors.* 2009;9(3):1967-1979.
11. Straub J, Kerlin S. Development of a Large, Low-Cost, Instant 3D Scanner. *Technologies.* 2014;2(2):76-95.
12. Zingoni A, Diani M, Corsini G, Masini A. REAL-TIME 3D RECONSTRUCTION FROM IMAGES TAKEN FROM AN UAV. *International Archives of the Photogrammetry, Remote Sensing & Spatial Information Sciences.* 2015;40.
13. Moons T, Van Gool L, Vergauwen M. 3D Reconstruction from multiple images. *Foundations and Trends in Computer Graphics and Vision.* 2009;4(4):287-404.
14. Rostami M, Michailovich O, Wang Z. Gradient-based surface reconstruction using compressed sensing. Paper presented at: 2012 19th IEEE International Conference on Image Processing; 30 Sept.-3 Oct., 2012; Orlando, FL, USA.
15. Agrawal A, Chellappa R, Raskar R. An algebraic approach to surface reconstruction from gradient fields. Paper presented at: Tenth IEEE International Conference on Computer Vision

(ICCV'05) Volume 1; 17-21 Oct. , 2005; Beijing, China.

16. Petrovic N, Cohen I, Frey BJ, Koetter R, Huang TS. Enforcing integrability for surface reconstruction algorithms using belief propagation in graphical models. Paper presented at: Proceedings of the 2001 IEEE Computer Society Conference on Computer Vision and Pattern Recognition. CVPR 2001; 8-14 Dec., 2001; Kauai, HI, USA.
17. Xie W, Zhang Y, Wang CC, Chung RC-K. Surface-from-gradients: An approach based on discrete geometry processing. Paper presented at: 2014 IEEE Conference on Computer Vision and Pattern Recognition; 23-28 June, 2014; Columbus, OH, USA.
18. Tomasi C, Manduchi R. Bilateral filtering for gray and color images. Paper presented at: Sixth International Conference on Computer Vision 7-7 Jan., 1998; Bombay, India.
19. Venkatesh M, Seelamantula CS. Directional bilateral filters. Paper presented at: 2015 IEEE International Conference on Acoustics, Speech and Signal Processing (ICASSP); 19-24 April, 2015; Brisbane, QLD, Australia.
20. Wang K, Torkhani F, Montanvert A. A fast roughness-based approach to the assessment of 3D mesh visual quality. *Computers & Graphics.* 2012;36(7):808-818.
21. Mesmoudi MM, De Floriani L, Magillo P. Discrete curvature estimation methods for triangulated surfaces. In: *Applications of Discrete Geometry and Mathematical Morphology.* Springer; 2012:28-42.
22. Sorkine O. Laplacian mesh processing. Paper presented at: Eurographics (STARs); 29 Aug.- 2 Sept., 2005; Dublin, Ireland.